NJC

New Journal of Chemistry

A journal for new directions in chemistry

Accepted Manuscript

This article can be cited before page numbers have been issued, to do this please use: B. Parshad, P. Yadav, Y. Kerkhoff, A. Mittal, K. Achazi, R. Haag and S. K. Sharma, *New J. Chem.*, 2019, DOI: 10.1039/C9NJ02612F.

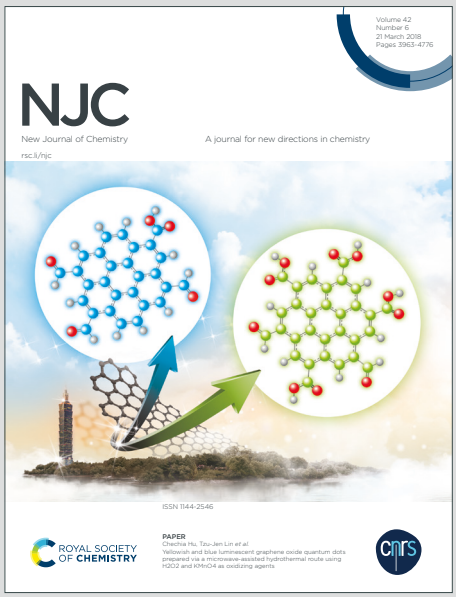

View Article Online
DOI: 10.1039/C9NJ02612F

Dendrimer-based Micelles as Cyto-compatible Nanocarriers

Badri Parshad,[a,b] Preeti Yadav,[a] Yannic Kerkhoff,[b] Ayushi Mittal,[a] Katharina Achazi,[b,*] Rainer Haag,[b] Sunil K. Sharma[a,*]

[a]*Department of Chemistry, University of Delhi, Delhi 110 007, India*

[b]*Institut für Chemie und Biochemie, Freie Universität Berlin, Takustraße 3, 14195 Berlin, Germany*

Abstract

A series of dendritic architectures have been synthesized using biocompatible materials such as glycerol, glucose, phloroglucinol, and alkyl chains of varied sizes to confer them aqueous solubility and to attain proper hydrophilic-hydrophobic balance allowing them to form nano-sized aggregates for the encapsulation and delivery of drugs/dyes for biomedical applications. The aggregation behavior of these dendritic architectures as well as cytotoxicity and their cellular uptake were studied using fluorescence measurements, dynamic light scattering (DLS), transmission electron microscopy (TEM), live cell imaging by confocal laser scanning microscopy (cLSM), and flow cytometry. Aggregation study has shown that dendrimers proficiently self-assemble in aqueous solution with low micromolar concentration and form uniformly spread micellar aggregates. The effective cellular uptake of Nile red loaded into the dendrimers as well as the very low toxicity of the dendrimers points out their potential as carriers for drugs and imaging agents.

Keywords: cellular internalization, cytotoxicity, dendrimers, micelles, self-assembly

View Article Online
DOI: 10.1039/C9NJ02612F

Introduction

Reduced or limited drugs' potency and therapeutic effects due to low aqueous solubility, non-specific binding, poor cell membrane permeability, and partial degradation are the various hurdles that the researchers across the world are attempting to address. To achieve the goal of a target-specific delivery of drugs with improved pharmacokinetic profile, researchers are turning to nanocarrier systems. In order to accomplish the discovery of new nanostructures and drug delivery agents, numerous studies have been carried out.[1-8] Among the many nanoparticulate drug delivery systems being studied, the use of dendritic macromolecular systems as an efficient drug delivery agent has attracted significant attention in recent years.[9,10] Appropriate control over dendritic architectures (size, shape, and solubility) and multiple functionalities at the surface make dendrimers potential building blocks for the fabrication of efficient functional materials for drug delivery applications.[11] In comparison to linear amphiphiles, dendrimers lead to the formation of stable micelles as they possess a well-defined shape with multiple branching that makes them dense enough to prevent reverse micellization by inverting the branches. This stability enhances the duration of their circulation in blood and reduces the risk of premature clearance of encapsulated drug from the body with reproducible pharmacokinetic behavior.[12] The use of dendrimers for drug encapsulation and transport has extensively been reviewed by many research groups.[13-15] Encapsulation of small molecules including naphthalocyanine,[16] pyrene,[17] and phenol blue[18] within poly(aryl ether), polyester, or poly(amido amine) dendrimer has also been reported and there is much more to explore in this field. To further explore the dendritic architecture as drug delivery vehicles and their self-assembly in aqueous medium, herein, a series of dendritic architectures were synthesized that employed the divergent approach and used the symmetrical aromatic core of phloroglucinol, which not only reduced crowding but also imparted π-π interactions, a driving force for the encapsulation of aromatic guest molecules. In order to render aqueous solubility to the synthesized dendrimers, biocompatible materials such as glycerol and D-glucose were used. Furthermore, to enhance the flexibility and hydrophobicity, longer alkyl chains were incorporated that can facilitate the creation of interior hydrophobic cavity in the aggregates formed in aqueous medium. In an attempt to attain micellar stability as well as to maximize the transport potential of guest molecules, hydrophobic-hydrophilic balance was optimized via the use of different types of hydrophilic/hydrophobic units. The aggregation of these dendritic architectures in an aqueous medium to form micelles/micellar aggregates might be due to

View Article Online
DOI: 10.1039/C9NJ02612F

the formation of tripod like structures, allowing the efficient interaction between hydrophobic and hydrophilic units in an individual manner. As a consequence of these interactions, the hydrophobic core/branching are directed in the interior of the aggregates forming a hydrophobic cavity, with the hydrophilic surface groups directed towards the exterior (**Figure 1**). The main cause of encapsulation of hydrophobic entities is hydrophobic interactions between micellar core and encapsulated molecules. Moreover, π-π stacking is also possible between the dendrimer aromatic core and the π-electron cloud of the guest molecules. The self-assembling behavior of the resulting dendrimers was studied by using dynamic light scattering (DLS), transmission electron microscopy (TEM), and critical aggregation concentration (CAC) measurements, which facilitated a comparison of the resulting D-glucosyl/glyceryl and alkylated dendritic architectures. The synthesized dendritic systems were investigated for their transport potential using model hydrophobic compounds like the dye Nile red and the biologically potent molecule curcumin. The dendrimers exhibiting good encapsulation potential were further investigated for their cytotoxicity and cellular internalization using adenocarcinomic human alveolar basal epithelial A549 cells.

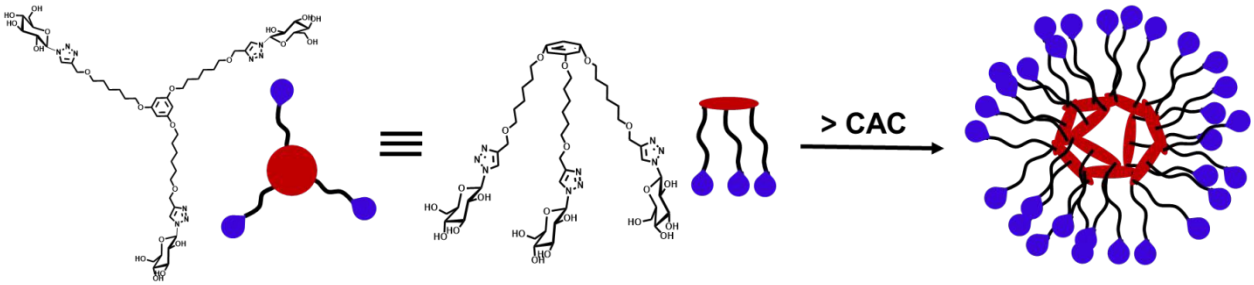

Figure 1. Proposed schematic representation of dendritic micellar aggregates in aqueous medium.

Experimental Section

NMR, IR, and Mass analysis

^{1}H and ^{13}C NMR spectra were recorded on Jeol-400/100.5 MHz spectrometer, respectively, using the solvent residual peak as a reference, where the chemical shift values are on a δ scale and the coupling constant values (*J*) are taken in Hertz. Infrared (IR) spectra and the HRMS data of the compounds were recorded on a Perkin-Elmer 2000 FT-IR spectrometer and Agilent-6530, Q-TOF LCMS, respectively.

Critical Aggregation Concentration (CAC) Measurement

View Article Online
DOI: 10.1039/C9NJ02612F

Nile red, a model hydrophobic dye, was used as a probe to determine the CAC of the dendrimers by fluorescence measurements.[19] A stock solution of 1 mg/mL of Nile red in THF (1 mL) was prepared and 50 μL of this stock solution were taken in empty vials and THF was allowed to evaporate completely. Different concentrations of dendrimers (3 mM to 0.73 μM) were prepared (2 mL) and added sequentially in the vials that had Nile red. The solution was stirred overnight, the non-encapsulated dye was removed by a 0.45 μm polytetrafluoroethylene (PTFE) filter, and the solution was subjected to fluorescence measurements. The CAC value was calculated by plotting the fluorescence intensity maxima against the log[dendrimer] concentration.

Dynamic Light Scattering (DLS) and Transmission Electron Microscopy (TEM)

The size of the nanoparticles was measured by DLS using Malvern Zetasizer Nano ZS analyzer integrated with 4 mW He-Ne laser, $\lambda = 633$ nm, using backscattering detection (scattering angle $\theta = 173°$). An aqueous solution of dendrimers (3 mg/mL) transferred into disposable cuvettes was used for measurements. Because of their limited solubility, dendrimers **13** and **16** formed turbid solution. The nanoparticles formed were further analyzed by transmission electron microscopy (TEM) using a TECNAI G2-30 U-TWIN TEM instrument (FEI, Eindhoven, The Netherlands) with an acceleration voltage of 200 kV. The sonicated aqueous solution of the sample was drop-coated and dried onto formvar-coated 200 mesh copper grids (Ted Pella, USA) and analyzed by TEM.

Procedure for Nile red and curcumin encapsulation

For Nile red encapsulation, a stock solution of 1 mg/mL of Nile red in THF (1 mL) was prepared. 50 μL of the stock solution was transferred in a vial and evaporated to dryness to form a thin film (film method)[20] followed by the addition of 1 mL of an aqueous solution of dendrimer (3 mg/mL). The resulting solution was stirred overnight. For quantification of Nile red, a known amount of the sample was lyophilized and re-dissolved in methanol for absorbance measurement and the amount of encapsulated dye was calculated employing Lambert-Beer's law and using Nile red's molar extinction co-efficient (ε) of 45,000 $M^{-1}cm^{-1}$ at 552 nm.[21]

Curcumin encapsulation was carried out using a solid dispersion method,[22] wherein, 1 mg of curcumin dissolved in a minimum amount of methanol was mixed with the methanolic solution of dendrimer (3 mg/mL). The mixture was evaporated to dryness under reduced pressure followed by the addition of 1 mL of water and stirred for overnight. The quantification of encapsulated

View Article Online
DOI: 10.1039/C9NJ02612F

curcumin was done following the same method as used for Nile red and using the molar extinction co-efficient (ε) of 55,000 $M^{-1}cm^{-1}$ at 425 nm for curcumin in methanol.

Cellular uptake study

Cellular uptake of Nile red-encapsulated dendritic systems in A549 cells (ACC 107, DSMZ, The Leibniz Institute DSMZ-German Collection of Microorganisms and Cell Cultures GmbH, Braunschweig, Germany) was monitored by confocal laser scanning microscopy (cLSM) and flow cytometry. The cells were routinely propagated in DMEM medium supplemented with 2% glutamine, 100 U/mL penicillin, 100 µg/mL streptomycin (all from Gibco BRL, Eggenstein, Germany), and 10% fetal calf serum (Biochrom AG, Berlin, Germany) at 37 °C with 5% CO_2, and subcultured twice a week. The Nile red encapsulated dendritic architectures were prepared by incubating the dye in an aqueous solution of dendrimer using the film method at a concentration of 5 mg/mL.

For cLSM, cells were seeded in 8-well ibidi µ-slides (27.000 cells/well) in colorless cell culture medium. After 1 day, the compounds were added at a final test concentration of 0.5 mg/mL and incubated for either 30 min, 5 h, or 24 h. For staining of endocytotic compartments, Cell Light GFP reagents (Life Technologies GmbH, Darmstadt, Germany) were used according to the manufacturer's instructions to specifically label either early endosomes (CellLight™ Early Endosomes-GFP, BacMam 2.0) or lysosomes (CellLight™ Lysosomes-GFP, BacMam 2.0) in cells incubated for 5 h with the encapsulated dye. Non-treated either labeled or non-labeled cells served as control to adjust the settings. Confocal images of the living cells were taken with an inverted confocal laser scanning microscope Leica DMI6000CSB SP8 (Leica, Wetzlar, Germany) with a 63x/1.4 HC PL APO CS2 oil immersion objective using the manufacture-given LAS X software. If not stated elsewhere, all the images were taken using the same settings to ensure that the fluorescence intensity between the different images and times can be compared. Images analysis was performed using a self-written ImageJ Macro. To determine the single-cell fluorescence signal, the image stack was smoothed and then the background (threshold value > 5) was excluded and the remaining pixel converted to a binary mask. On the resulting binary images, different morphological operators were applied (despeckle, close, fill holes, dilate, erode) to reduce remaining noise, fill the holes from the nucleus and reshape the cell borders. Then, a watershed algorithm with a tolerance of 2 was applied to separate cells close to each other. The resulting

View Article Online
DOI: 10.1039/C9NJ02612F

binary mask was superimposed on the original image series to mask all the background noise and separate the cells while preserving the original fluorescence signal. The mean fluorescence intensity of each cell was automatically analyzed by ImageJ's Particle Analyzer function and the mean intensity of all cells per frame was calculated. The data was then plotted using Origin.

For flow cytometry, cells were seeded in 24-well plates (100.000 cells per well). After 1 day, the Nile red loaded compounds were added at a final test concentration of 0.5 mg/mL and the cells were incubated at either 37 °C or 4 °C for another 10 min or 30 min, respectively. Cells were detached by trypsin, transferred to an Eppendorf tube, centrifuged at 140 xg and 4 °C for 4 min, and resuspended in PBS. Fluorescence of the cells was measured in a BD Accuri C6 (Becton Dickinson, Heidelberg, Germany) and analysis was done by the FlowJoe software. Data was plotted with the Origin software.

The uptake profile of compound **14** loaded with Nile red (**14**/NR) at a final concentration of 0.5 mg/mL was compared to free Nile red (NR) by confocal laser scanning microscopy (cLSM and flow cytometry) using A549 cells. The concentration of free NR was adjusted to the same concentration loaded onto **14**. cLSM images were taken from living A549 cells incubated for 30 min with **14**/NR or free NR and the data was analyzed to generate the resulting time-dependent uptake profile. For a quantitative analysis, ten images per sample were taken after 10 min and 30 min and the mean with SD was plotted for each sample. For the imaging and following time-lapse analysis cells were placed under a confocal laser scanning microscope and excited at 651 nm with 0.1% laser intensity every 2.6 sec. Fluorescence was detected between 570 nm and 751 nm with a photomultiplier (PMT). In the images, Nile red is shown in red color. For the quantitative analysis, laser intensity was increased for free NR to 1% and remained for **14**/NR at 0.1% to prevent over saturation. By using images made at both laser intensities, the data was normalized. For the time-dependent visualization and the quantitative analysis, the highest signal was set to 1 and all other values were normalized accordingly. Flow cytometry was used additionally for quantitative analysis of the uptake of **14**/NR and NR in A549 cells and to compare the uptake efficiency and at 4 °C and 37 °C. About 10,000 cells were counted per experiment and analyzed plotting the mean with SD of two independent experiments. Cells were excited at 633 nm and fluorescence was detected using a LP750 filter using Accuri C6 flow cytometer (BD).

View Article Online
DOI: 10.1039/C9NJ02612F

Results and Discussion

Synthesis and characterization

Initially the dendritic synthons like azido glycerol, glucose azide, alkyne, etc., were synthesized by the already reported procedures using easily available biocompatible materials such as glycerol, glucose, and phloroglucinol.[23-26] The dendrimers were synthesized by following a divergent approach using click and Williamson synthesis reactions (**Schemes 1-4**). All the synthesized dendrimers were characterized by IR, ^{1}H NMR, and ^{13}C NMR, and the final dendrimers were also characterized by their HRMS analysis. The characteristic peak of the three triazolyl protons (H-5") of dendrimer **3** appeared at δ 8.17 ppm as a singlet and the peak for the six methylene protons (H-1') attached to the triazole moiety appeared as a singlet at δ 5.03 ppm (**Figure S3, ESI**). Similarly, for dendrimer **4**, the respective peaks for the triazolyl ring (H-5") and the methylene protons (H-1') appeared at δ 8.02 and δ 4.81 ppm, respectively (**Figure S4, ESI**). For the second-generation dendrimer **6,** the two singlets at δ 7.96 and 8.23 ppm for the six and three protons, respectively, were from the external (H-c) and internal (H-5") triazolyl ring, respectively (**Figure S9, ESI**). In the case of dendrimer **7**, both the triazolyl ring protons (H-5" & H-c) appeared as a multiplet in the range δ 7.81-7.80 ppm (**Figure S10, ESI**). For the modified G1 dendrimer **13,** the peak at δ 8.00 ppm accounts for the triazole protons (H-5"') that appeared at δ 7.93 ppm for dendrimer **14**. Similarly, second-generation modified dendrimers **16** and **17** were characterized by their NMR and mass spectra. The final deprotection of all the acetyl-protected dendrimers was also confirmed by the disappearance of the ester carbonyl (-C=O) peak at ≈1740 cm^{-1} in the IR spectra.

View Article Online
DOI: 10.1039/C9NJ02612F

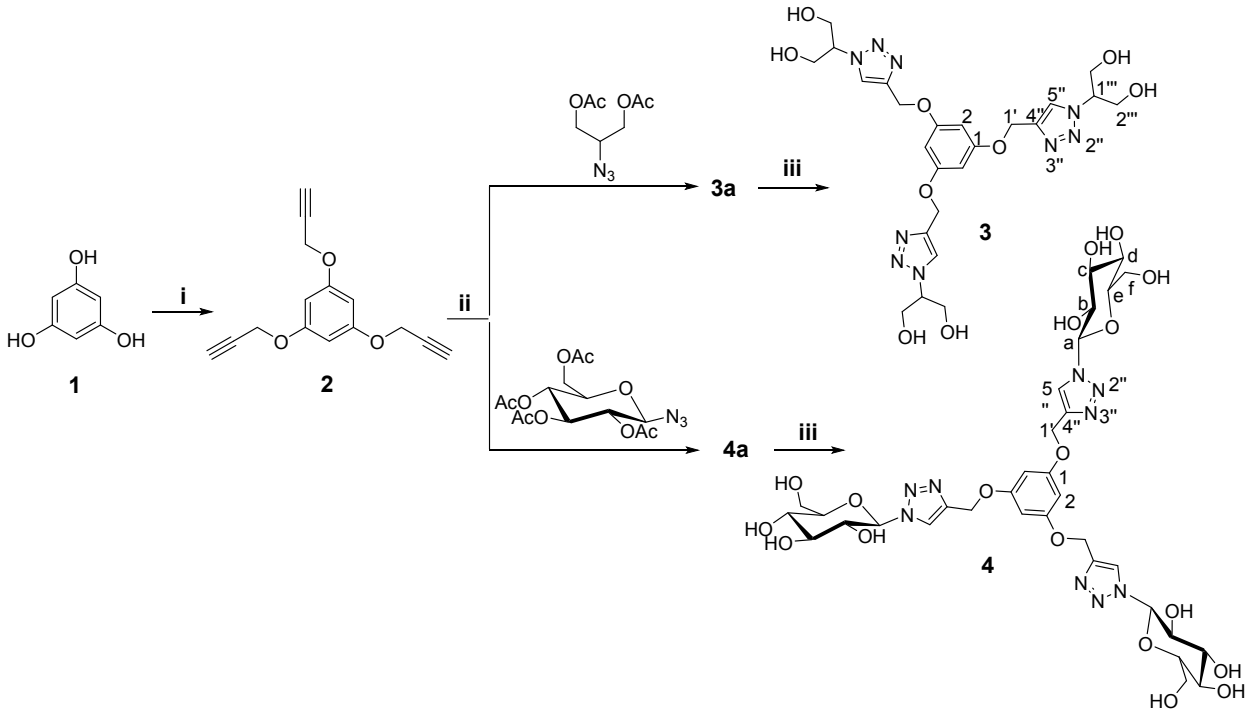

Scheme 1. Synthesis of first-generation (G1) dendrimers **3** and **4**: (i) propargyl bromide, K_2CO_3, DMF; (ii) $CuSO_4.5H_2O$, sodium ascorbate, THF:H_2O (3:1), 45 °C; (iii) 1N NaOH in methanol, Dowex 50WX8.

View Article Online
DOI: 10.1039/C9NJ02612F

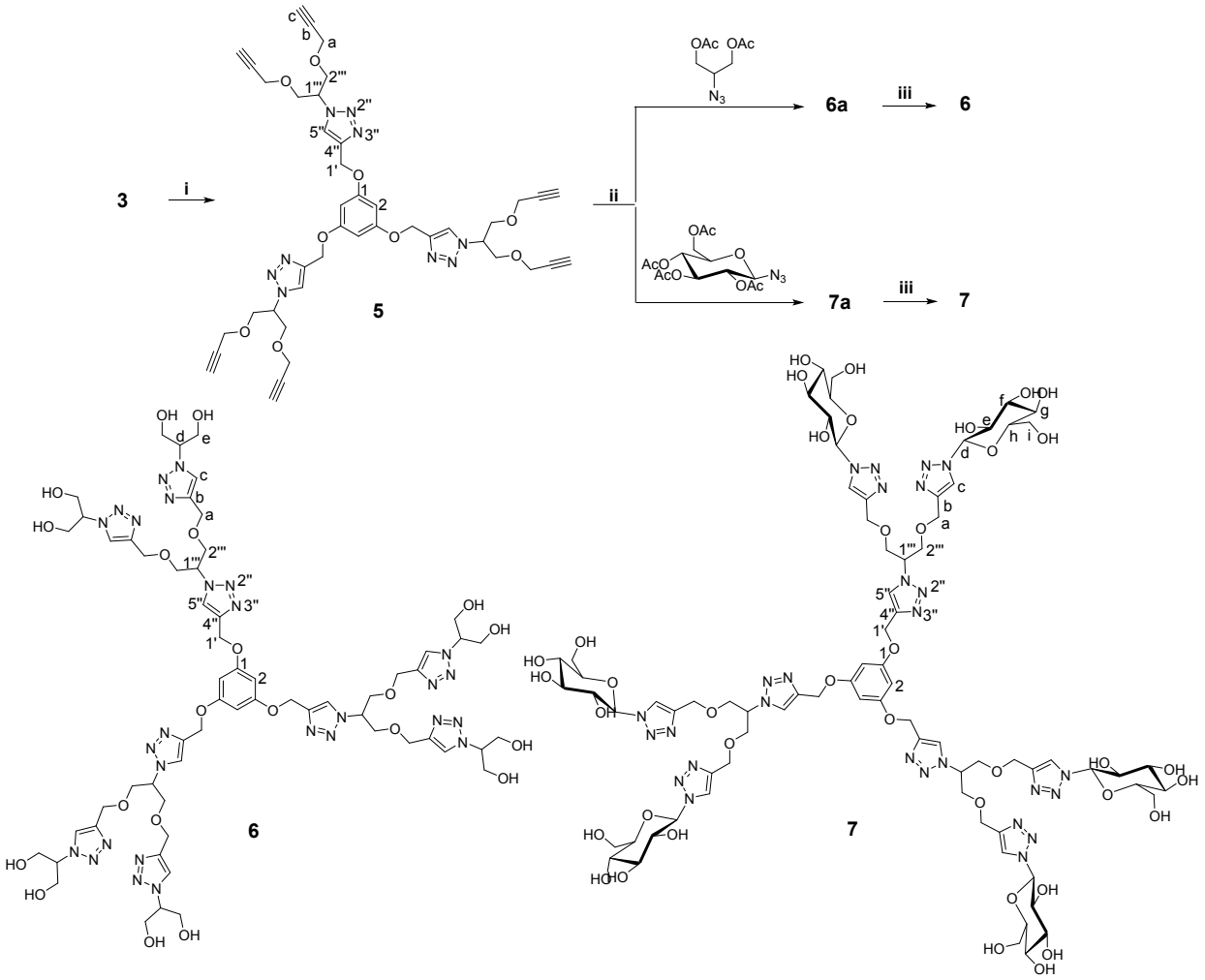

Scheme 2. Synthesis of second-generation (G2) dendrimers **6** and **7**: (i) propargyl bromide, NaOH, TBAI, H_2O; (ii) $CuSO_4.5H_2O$, sodium ascorbate, THF:H_2O (3:1), 45 ^oC; (iii) 1N NaOH in methanol, Dowex 50WX8.

View Article Online
DOI: 10.1039/C9NJ02612F

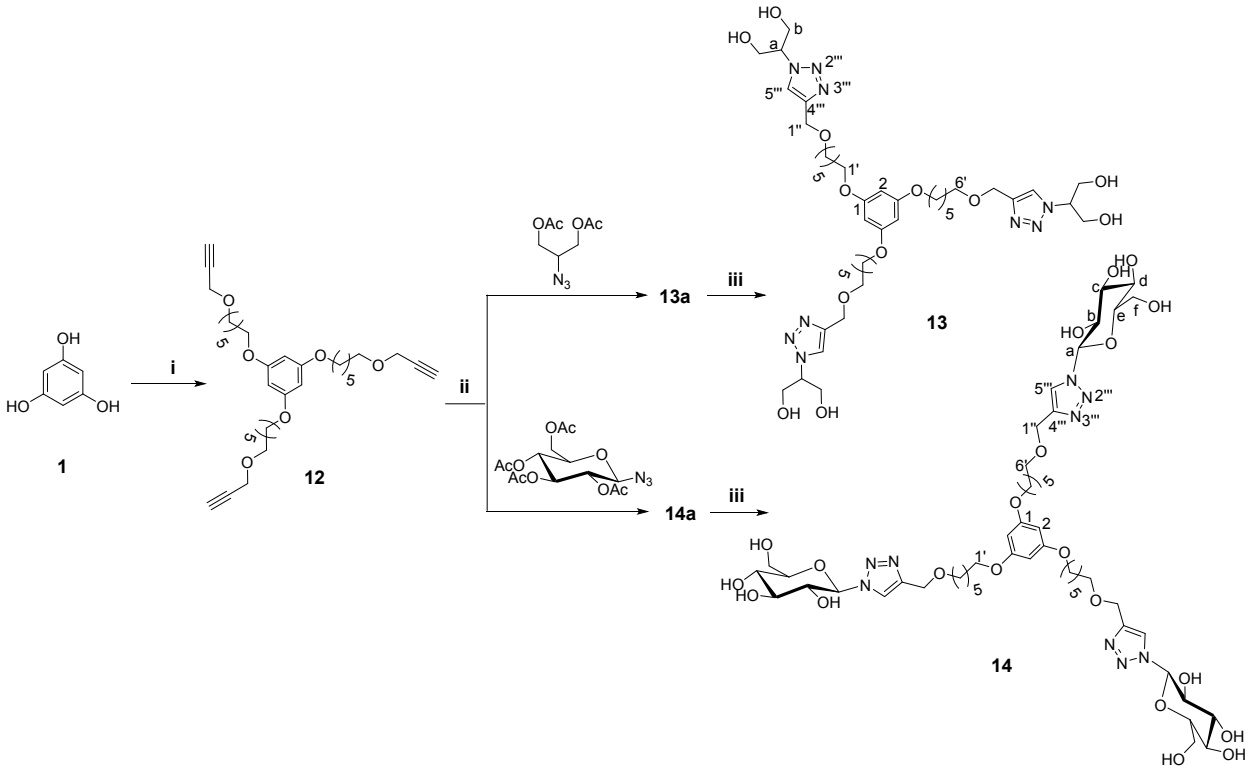

Scheme 3. Synthesis of alkylated first-generation (alkylated G1) dendrimers **13** and **14**: (i) 1-bromo-6-(prop-2-yn-1-yloxy)hexane (**10**), K_2CO_3, DMF; (ii) $CuSO_4.5H_2O$, sodium ascorbate, THF:H_2O (3:1), 45 ^oC; (iii) 1N NaOH in methanol, Dowex 50WX8.

View Article Online
DOI: 10.1039/C9NJ02612F

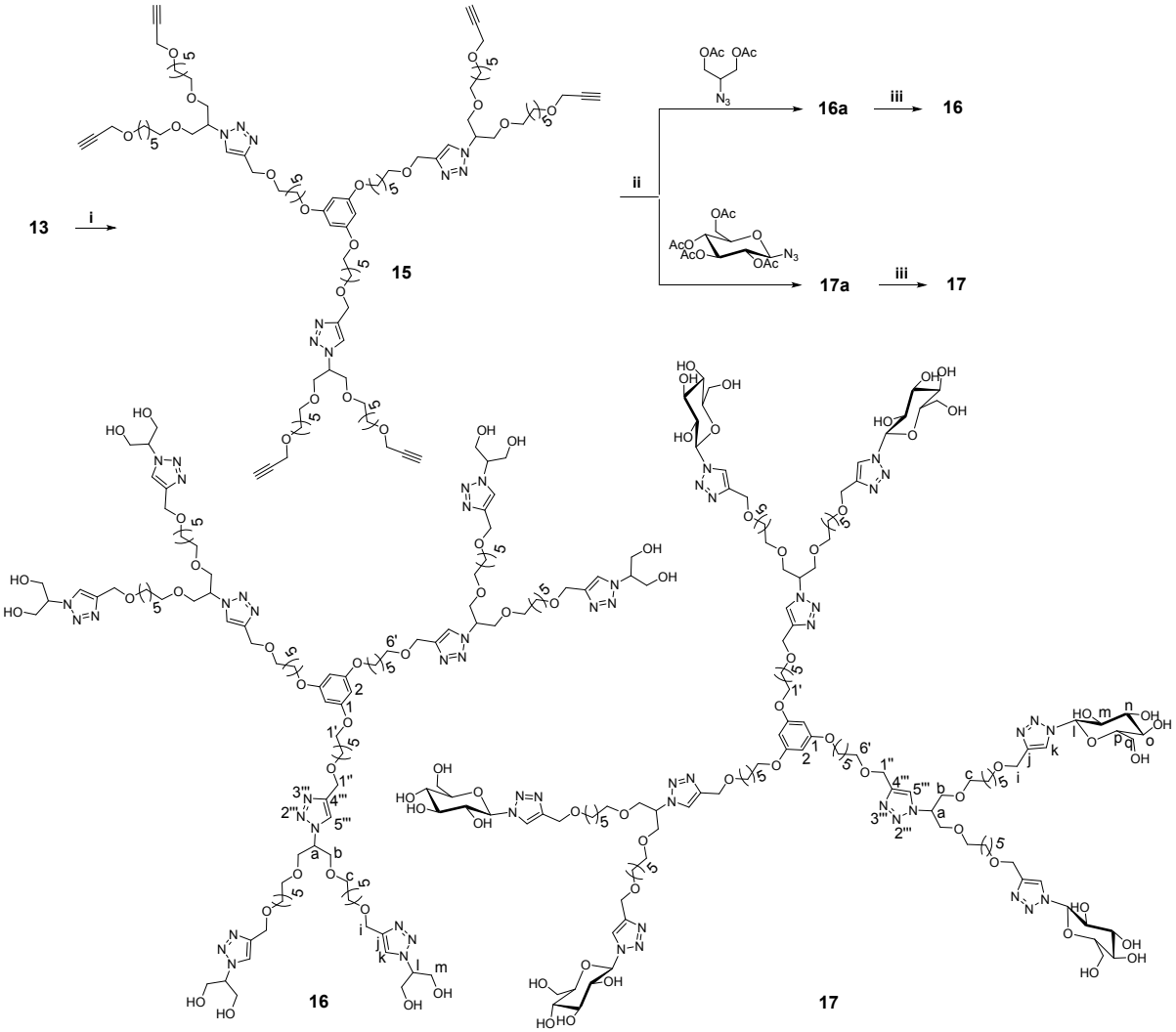

Scheme 4. Synthesis of alkylated second-generation (alkylated G2) dendrimers **16** and **17**: (i) 1-bromo-6-(prop-2-yn-1-yloxy)hexane, NaOH, TBAI, H_2O; (ii) $CuSO_4.5H_2O$, sodium ascorbate, THF:H_2O (3:1), 45 ^oC; (iii) 1N NaOH in methanol, Dowex 50WX8.

CAC measurement

The CAC of an aqueous solution of the self-assembled dendrimers (**13**, **14**, **16**, and **17**) was determined using Nile red as a fluorescent probe,[27] wherein a fixed amount of dye was used for encapsulation in different concentrations of dendrimers. The dye exhibited low fluorescence intensity in the absence of the supramolecular structure and an increase observed at a specific concentration, which indicated its encapsulation within the self-assembled nanostructures. The intensity maxima (λ_{max}) of encapsulated Nile red plotted versus log[dendrimer] was used to calculate the CAC value of the dendrimers. The dendrimers **3**, **4**, **6**, and **7** that lack a flexible C_6 alkyl chain were found to exhibit an irregular

View Article Online
DOI: 10.1039/C9NJ02612F

pattern for Nile red encapsulation, hence their CAC analysis could not be satisfactorily performed. However, the dendritic systems bearing C_6 alkyl chain displayed systematic encapsulation behavior, with CAC values observed to be in the order of 10^{-5} M (**Figure 2** & **Table S1, ESI**). A comparison of the CAC values of the modified G2 dendrimers (**16** and **17**) with their respective G1 analogs (**13** and **14**) revealed that the increase in dendrimer generation resulted in lower CAC values. This might be attributed to higher hydrophobic and hydrophilic contents in the higher generation dendrimers, facilitating them to aggregate at low concentration. **Figure 1** shows the proposed schematic representation of aggregation phenomenon in aqueous solution. Zhang et al. also investigated the similar type of self-aggregation of amphiphilic dendrimers into various morphologies including vesicular structures in aqueous medium by varying the alkyl chain length on periphery.[28]

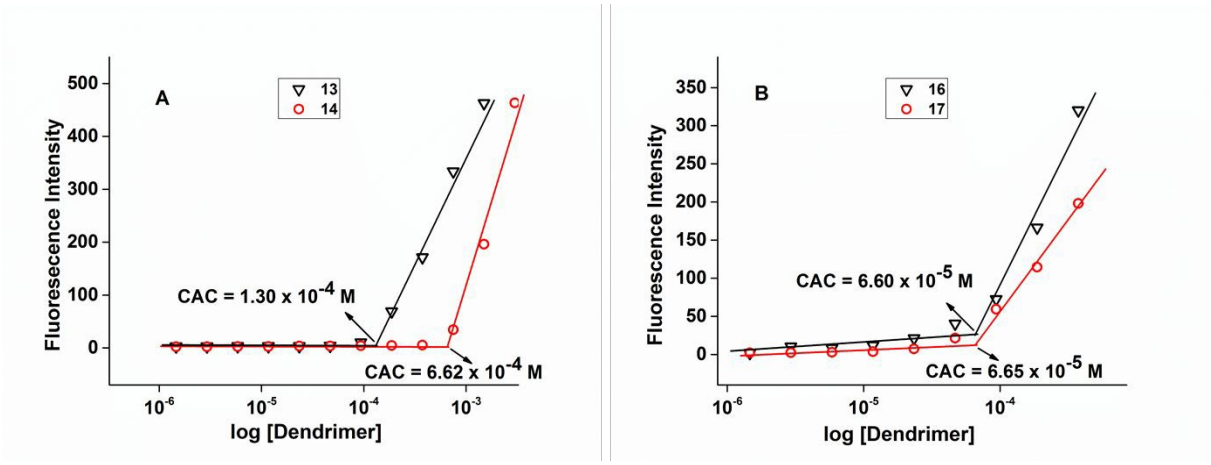

Figure 2. CAC measurements of (A) dendrimers **13** & **14** and (B) dendrimers **16** & **17**.

DLS and TEM analysis

The aggregation phenomenon of the synthesized dendrimers (**3**, **4**, **6**, **7**, **13**, **14**, **16**, and **17**) was studied in aqueous medium by DLS measurements at a concentration of 3 mg/mL (**Figure 3** & **Table S1**, **ESI**). The dendrimers **3**, **4**, **6**, and **7** that lack flexible alkyl chains were found to exhibit an irregular pattern in DLS, hence their size could not be measured. The dendrimers **14**, **16**, and **17** exhibited size of 7-8 nm indicating defined micellar aggregates, however, the dendrimer **13** aggregated into larger sized particles of 0.7 µm.

View Article Online
DOI: 10.1039/C9NJ02612F

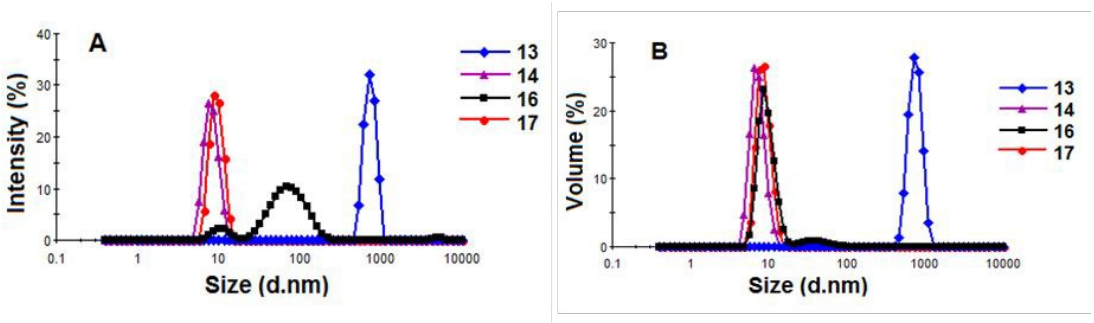

Figure 3. DLS size distribution plots (A) by intensity distribution and (B) by volume distribution, of dendrimers **13**, **14**, **16**, and **17**.

According to literature reports, smaller nanoparticles in the range of 8-20 nm not only can easily penetrate the deep regions of interstitial tissue but also circumvent the rapid renal clearance.[29] Thus the size of the self-assembled dendritic systems **14**, **16**, and **17** appear to be quite appropriate for the transport of drugs. However, the dendrimers **3**, **4**, **6**, and **7** did not exhibit the formation of stable and particular sized aggregates as evidenced by DLS study. This might be the consequence of a poor hydrophilic-lipophilic balance.[30]

In order to further investigate the morphology of the micellar aggregates, a TEM study was carried out for two selected dendrimers **14** and **17** (**Figure 4**). The results obtained from TEM were found to be consistent with that obtained from DLS with slight variation in size. In TEM study, different sized particles can be seen with size in the range of 5 to 15 nm for the dendrimers **14** and **17**, while in DLS an average size of around 8 nm was observed for both.

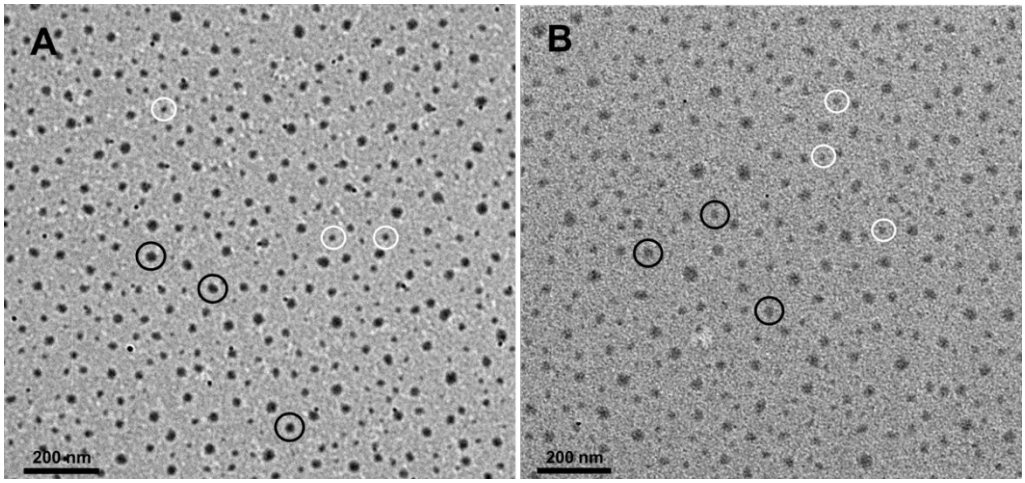

Figure 4. TEM images of (A) dendrimer **14** and (B) dendrimer **17**, showing spherical micellar assemblies (black circles in both images indicate the size of around 15 nm and white circles indicate the size of around 5 nm).

View Article Online
DOI: 10.1039/C9NJ02612F

Transport potential of dendrimers for Nile red and curcumin

Nile red, a fluorescent hydrophobic probe that is used for the recognition of the neutral lipid deposit within the cells,[31] was used to assess the transport behavior of the synthesized dendrimers. The applicability of these new dendritic systems as nanocarriers was explored by performing drug/dye solubilization experiments. The encapsulation potential of the dendrimers **13**, **14**, **16**, and **17** was determined for two exemplary hydrophobic entities, the dye Nile red and the biologically potent molecule curcumin. The fluorescence spectra of Nile red and curcumin loaded samples in methanol are shown in **Figure 5** while UV absorbance spectra for the same are shown in **Figures S23 and S24**, **ESI**. The C_6 alkylated G2 dendrimer **17** bearing glucosyl moiety at the periphery showed the highest encapsulation of Nile red, with a transport efficiency of 4.56 mg/g as shown in **Figure 6** and **Table 1**. On the other hand, 1 g of dendrimer **13**/**14**/**16** was able to transport 0.59/1.32/3.93 mg of Nile red, respectively. The non-alkylated dendrimers (**3**, **4**, **6**, and **7**) do not exhibit any noticeable absorbance for Nile red in UV-Vis spectra up to the measured concentration.

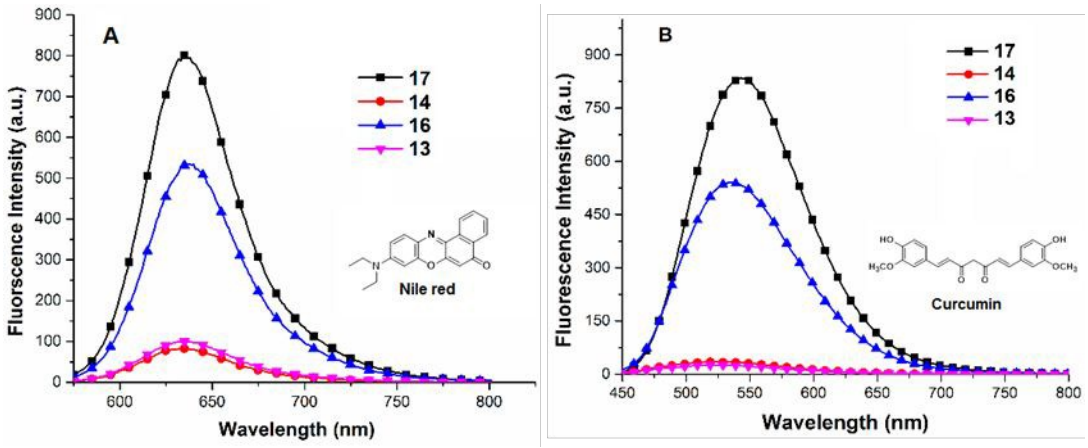

Figure 5. Fluorescence spectra in methanol for (A) Nile red and (B) curcumin loaded samples.

Curcumin, a hydrophobic drug, used as a dietary supplement in Southeast Asia and having versatile biological and pharmacological activities such as anticancer, antioxidant, antimicrobial, anti-parasitic, etc., but it has not been used clinically because of its poor aqueous solubility and low permeability across the blood-brain barrier which cause poor oral and brain bioavailability.[32-34] Nanocarriers can help to overcome these hurdles by making it water dispersible. Therefore, the synthesized dendrimers (**13**, **14**, **16**, and **17**) were used to investigate the encapsulation potential using curcumin. Among the studied dendrimers, the second-generation modified dendrimers **16**

View Article Online
DOI: 10.1039/C9NJ02612F

and **17** exhibited significant potential for the successful transportation of curcumin. On the other hand, negligible curcumin encapsulation was observed for the C_6 alkylated G1 dendrimers **13** and **14**. The low encapsulation of curcumin by the dendrimers **13** and **14** might be due to the difficulty of rigid and larger sized curcumin to fit in the small cavity/voids formed by these G1 dendrimers. The transport efficiency of the dendrimers **16** and **17** for curcumin was found to be 8.78 and 9.0 mg/g, respectively (**Figure 6** and **Table 1**). Jansen et al.[35-38] studied the cavity size-based encapsulation of hydrophobic molecules into dendrimers. They reported that large guest molecules (Rose Bengal) were encapsulated in the larger interior cavities, while the smaller ones (*p*-nitrobenzoic acid) were transported to the smaller outer cavity of the G5-PPI dendrimer.

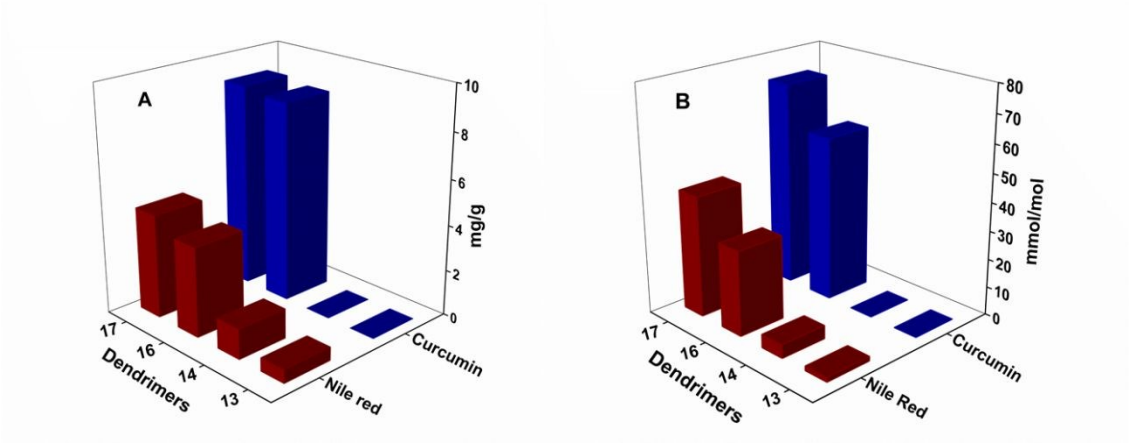

Figure 6. (A) Transport efficiency and (B) transport capacity of dendrimers **13**, **14**, **16**, and **17** for Nile red and curcumin.

Table 1. Transport behavior of dendrimer for the hydrophobic molecules Nile red and curcumin.

Dendrimer	Transport Behavior			
	Nile red/Polymer		Curcumin/Polymer	
	mg/g	mmol/mol	mg/g	mmol/mol
13	0.59	1.65	-	-
14	1.32	4.78	-	-
16	3.93	29.9	8.78	57.84
17	4.56	42.6	9.0	72.19

Biological characterization

As the compounds showed only very low toxicity in A549 cells (**Figure S26**, **ESI**), live cell imaging by confocal laser scanning microscopy (cLSM) as well as flow cytometry was used to

View Article Online
DOI: 10.1039/C9NJ02612F

analyze the uptake profile of Nile red loaded into dendrimers using adenocarcinomic human alveolar basal epithelial (A549) cells.

In a first approach, the uptake of two selected compounds **14** and **17** in A549 lung cancer cells was analyzed by cLSM. Microscopy images revealed Nile red uptake in the cells and accumulation over time (**Figure S27**, **Video S1** and **S2**, **ESI**). In the cell, Nile red was located not only in endocytotic compartments (lysosomes and early endosomes) but also in the cytoplasm around the nucleus. No Nile red was seen in the nucleus. The results indicated a non-endocytotic continuous uptake of the encapsulated Nile red as described earlier by Snipstad et al.[39] To confirm passive diffusion as a most relevant uptake mechanism for Nile red loaded in dendrimers, we further analyzed compound **14** and compared it to free Nile red using time-lapse microscopy combined with advanced image analysis and flow cytometry at 4 °C and 37 °C. Because active uptake, such as endocytosis is energy driven, the cellular uptake should be decreased at 4 °C. The flow cytometry data (**Figure 7**) revealed the passive diffusion mechanism as there was hardly any difference between the Nile red uptake at 4 °C and 37 °C. Time-lapse analysis combined with quantitative image analysis and the flow cytometry data further proved that the dendrimer was responsible for the efficient uptake of Nile red.

In summary, we assume that Nile red enters the cell by contact-mediated transfer as described earlier by Snipstad et al.[39] in which the carrier transports the guest to the target site (cells) by interaction with the cells. By this uptake mechanism, the hydrophobic drugs avoid the uptake via an endocytotic pathway and get direct access to intracellular targets.

View Article Online
DOI: 10.1039/C9NJ02612F

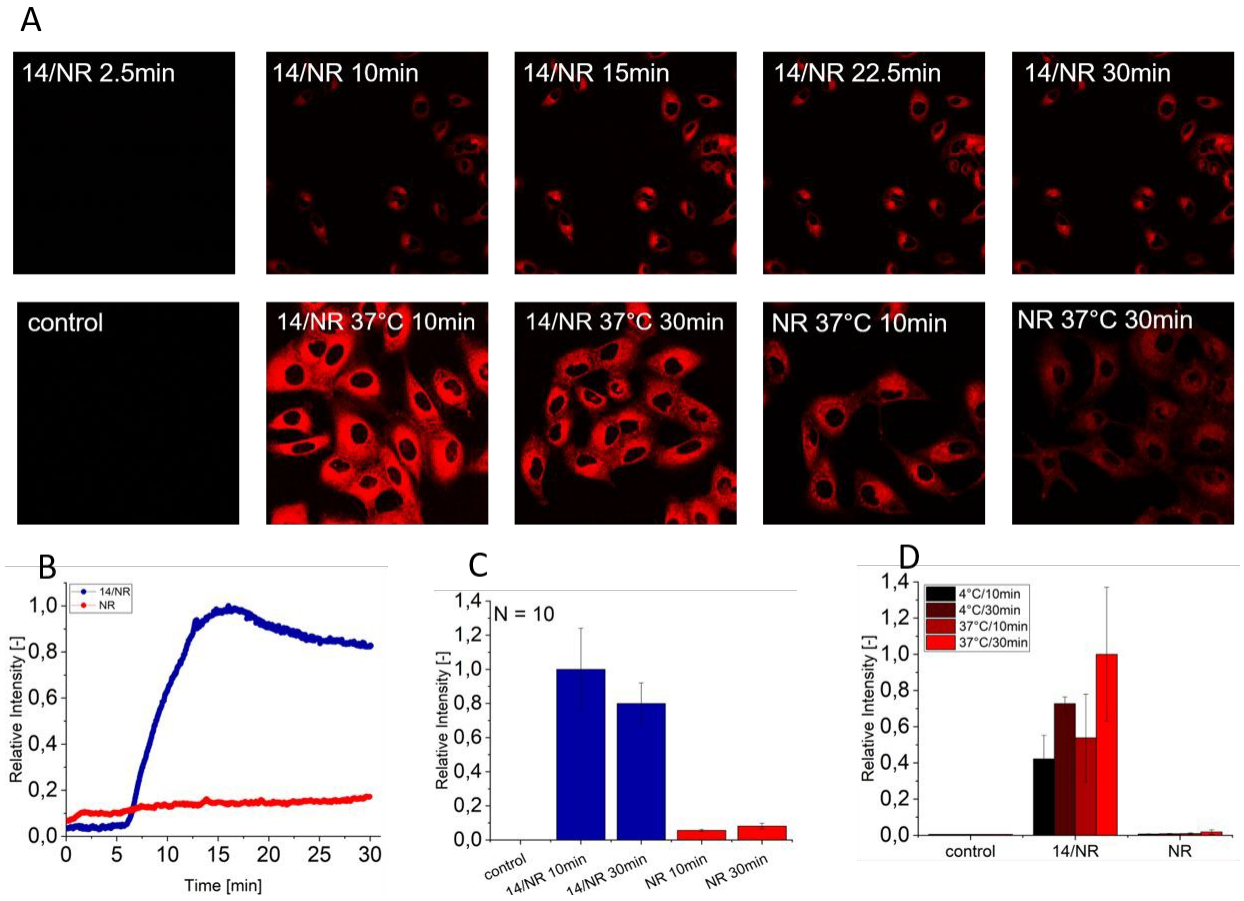

Figure 7. Uptake profile of compound **14** loaded with Nile red (**14**/NR) compared to free Nile red (NR) using A549 cells. (A) cLSM images from living A549 cells incubated for 30 min with **14**/NR or free NR; (B) the resulting time dependent uptake profile and (C-D) the quantitative uptake profiles; (C) based on the analysis of cLSM images and (D) based on flow cytometry measurements. In the images, Nile red is shown in red color.

Conclusions

We have prepared a series of dendritic architectures of different generations using biocompatible starting materials, i.e., D-glucose and glycerol. All of the dendritic architectures were characterized on the basis of their physical and spectral data. Of all the synthesized dendritic architectures, the C_6 alkyl chain containing dendrimers formed micellar aggregates in aqueous solution, with a CAC in the order of 10^{-5} M. DLS and TEM measurements confirmed that the dendrimers **14** and **17** formed stable and uniformly distributed micelles in the range of 5-15 nm. Furthermore, the modified G2 dendrimers having a larger hydrophobic cavity displayed the potential to solubilize curcumin and Nile red in water. The uptake study revealed efficient internalization of encapsulated Nile red

View Article Online
DOI: 10.1039/C9NJ02612F

inside the cancer cells, ascertaining the potential of the dendritic micelles to deliver the hydrophobic drug/dye by contact-mediated transfer inside the cells. The cytotoxicity profile obtained from MTS assay unraveled that the synthesized dendrimers exhibited toxicity only at higher concentrations, thus indicating their potential for drug delivery.

Acknowledgements: Financial assistance from DST-DFG collaborative research grant is gratefully acknowledged. Also, we are thankful to the Council of Scientific and Industrial Research (CSIR), New Delhi, for providing Junior/Senior Research Fellowships to BP, PY, and AM. We would like to acknowledge the assistance of the Core Facility BioSupraMol supported by the DFG.

References

1 C. Park, J. Lee and C. Kim, *Chem. Comm*., 2011, **47**, 12042.

2 Y. Chen, H. Zhou, Z. Sun, H. Li, H. Huang, L. Liu and Y. Chen, *Polymer,* 2018, **149**, 316-324.

3 S. Sabra, M. Abdelmoneem, M. Abdelwakil, M.T. Mabrouk, D. Anwar, R. Mohamed, S. Khattab, A. Bekhit, K. Elkhodairy, M. Freag and A. Elzoghby, *Curr. Pharm. Des.*, 2017, **23**, 1-17.

4 P. Calandra, D. Caschera, V.T. Liveri and D. Lombardoc, *Colloids Surf., A*, 2015, **484**, 164-183.

5 S. Prasad, K. Achazi, B. Schade, R. Haag and S.K. Sharma, *Macromol. Biosci.,* 2018, **18**, 1800019.

6 S. Prasad, K. Achazi, C. Böttcher, R. Haag and S.K. Sharma, *RSC Adv*., 2017, **7**, 22121-22132.

7 P. Chanphai and H.A. Tajmir-Riahi, *Mol. Cell Biochem.,* 2018, **449**, 157-166.

8 A.K. Singh, B.N.S. Thota, B. Schade, K. Achazi, A. Khan, C. Böttcher, S.K. Sharma and R. Haag, *Chem. Asian J*., 2017, **12**, 1796 -1806.

9 B.N.S. Thota, L.H. Urner and R. Haag, *Chem. Rev.*, 2016, **116**, 2079-2102.

10 F. Abedi-Gaballu, G. Dehghan, M. Ghaffari, R. Yekta, S. Abbaspour-Ravasjani, B. Baradaran, J.E.N. Dolatabadi and M.R. Hamblin, *Appl. Mater. Today,* 2018, **12**, 177-190.

11 A.V. Ambade, E.N. Savariar and S. Thayumanavan, *Mol. Pharm.,* 2005, **2**, 264-272.

12 S. Svenson, *Eur. J. Pharm. Biopharm.,* 2009, **71**, 445-462.

View Article Online
DOI: 10.1039/C9NJ02612F

13 M. Wyszogrodzka and R. Haag, *Chem. Eur. J.,* 2008, **14**, 9202-9214.

14 M.T. Morgan, Y. Nakanishi, D.J. Kroll, A.P. Griset, M.A. Carnahan, M. Wathier, N.H. Oberlies, G. Manikumar, M.C. Wani and M.W. Grinstaff, *Cancer Research,* 2006, **66**, 11913-11921.

15 M.T. Morgan, M.A. Carnahan, S. Finkelstein, C.A.H. Prata, L. Degoricija, S.J. Lee and M.W. Grinstaff, *Chem. Commun.,* 2005, 4309-4311.

16 O. Taratula, C. Schumann, T. Duong, K.L. Taylor and O. Taratula, *Nanoscale,* 2015, **7**, 3888-3902.

17 G. Pistolis and A. Malliaris, *Langmuir,* 2002, **18**, 246-251.

18 D.L. Richter-Egger, A. Tesfai and S. Tucker, *Anal. Chem.,* 2001, **73**, 5743-5751.

19 A.C. Rodrigo, A. Barnard, J. Cooper and D.K. Smith, *Angew. Chem. Int. Ed*., **2011**, *50*, 4675-4679.

20 E. Fleige, B. Ziem, M. Grabolle, R. Haag and U. Resch-Genger, *Macromolecules,* 2012, **45**, 9452-9459.

21 R.P. Haugland, Handbook of Fluorescent Probes and Research Chemicals, 6th ed., Molecular Probes Inc., Eugene, OR, USA, 1996.

22 V. Kumar, B. Gupta, G. Kumar, M.K. Pandey, E. Aiazian, V.S. Parmar, J. Kumar and A.C. Watterson, *J. Macromol. Sci., Pure Appl. Chem*., 2010, **47**, 1154-1160.

23 D. Bhunia, P. Pallavi, S.R. Bonam, S.A. Reddy, Y. Verma and M. Halmuthur, *Archiv der Pharmazie,* 2015, **348***,* 689-703.

24 S. Gupta, B. Schade, S. Kumar, C. Böttcher, S.K. Sharma and R. Haag, *Small*, 2013, **9**, 894-904.

25 C. Bayon, N. He, M. Deir-Kaspar, P. Blasco, S. Andre, H.J. Gabius, A. Rumbero, J. Jimenez-Barbero, W.D. Fessner and M.J. Hernaiz, *Chem. Eur. J.*, 2017, **23**, 1623-1633.

26 S. Chittabonia, F. Xie and Q. Wang, *Tetrahedron Lett.,* 2005, **46**, 2331-2336.

View Article Online
DOI: 10.1039/C9NJ02612F

27 A.C. Rodrigo, A. Barnard, J. Cooper and D.K. Smith, *Angew. Chem. Int. Ed*., 2011, **50**, 4675-4679.

28 P. Zhang, X. Xu, M. Zhang, J. Wang, G. Bai and H. Yan, *Langmuir,* 2015, **31**, 7919-7925.

29 V.P. Torchilin, *Nat. Rev. Drug Disc*., 2005, **4**, 145-160.

30 A. Sorrenti, O. Illa and R.M. Ortuno, *Chem. Soc. Rev.,* 2013, **42**, 8200-8219.

31 P. Greenspan, E.P. Mayer and S.D. Fowler, *J. Cell Biol.,* 1985, **100**, 965-973.

32 M.S. Cartiera, E.C. Ferreira, C. Caputo, M.E. Egan, M.J. Caplan and W.M. Saltzman, *Mol. Pharm*., 2010, **7**, 86-93.

33 A. Duvoix, R. Blasius, S. Delhalle, M. Schnekenburger, F. Morceau, E. Henry, M. Dicato and M. Diederich, *Cancer Lett.,* 2005, **223**, 181-190.

34 J.M. Ringman, S.A. Frautschy, G.M. Cole, D.L. Masterman and J.L. Cummings, *Curr. Alzheimer Res*., 2005, **2**, 131-136.

35 J.F.G.A. Jansen, E.M.M. de Brabander-van den Berg and E.W. Meijer, *Polym. Mater. Sci. Eng.,* 1995, **73**, 123-124.

36 J.F.G.A. Jansen and E.W. Meijer, *J. Am. Chem. Soc.,* 1995, **117**, 4417-4418.

37 J.F.G.A. Jansen, E.W. Meijer and E.M.M. De Brabander-van den Berg, *Macromol. Symp.,* 1996, **102**, 27-33.

38 J.F.G.A. Jansen, E.M.M. De Brabander-van den Berg and E.W. Meijer, *Science,* 1994, **266**, 1226-1229.

39 S. Snipstad, S. Westrom, Y. Morch, M. Afadzi, A.K. Aslund and C. de Lange Davies, *Cancer Nanotechnol.,* 2014, 5:8.

View Article Online
DOI: 10.1039/C9NJ02612F

Dendrimer-based Micelles as Cyto-compatible Nanocarriers

Badri Parshad,[a,b] Preeti Yadav,[a] Yannic Kerkhoff,[b] Ayushi Mittal,[a] Katharina Achazi,[b,*] Rainer Haag,[b] Sunil K. Sharma,[a,*]

[a]*Department of Chemistry, University of Delhi, Delhi 110 007, India*

[b]*Institut für Chemie und Biochemie, Freie Universität Berlin, Takustraße 3, 14195 Berlin, Germany*

Graphical Abstract

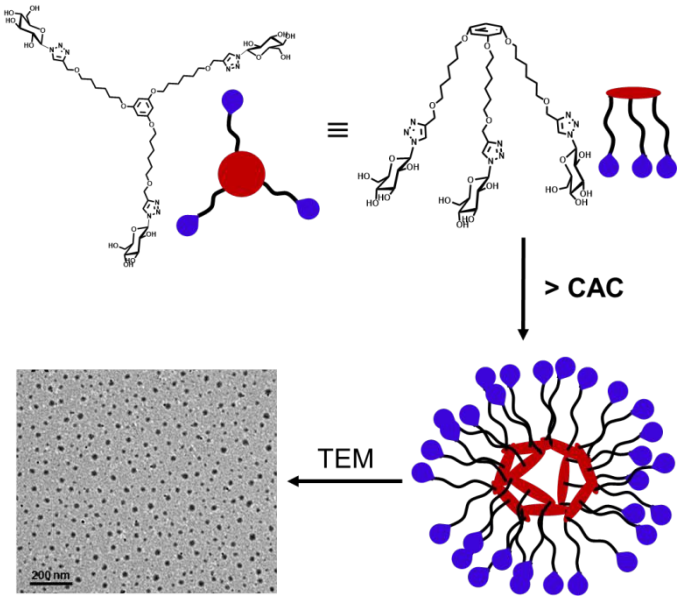

The aim of present study is to compare the synthesized dendritic architectures for self-assembly and transport potential for hydrophobic guest molecules.